# Mitigation of Ionospheric Noise in Azimuth Offset Based on the Split-Spectrum Method

Tatsuya Yamashita, Yu Morishita, and Tomokazu Kobayashi

***Abstract*— The pixel-offset method has been utilized as a powerful tool to measure large ground movements. However, L-band spaceborne synthetic aperture radar (SAR) data are often affected by the ionosphere, which produces serious noises in the azimuth component of the pixel offset field, called as azimuth streaks. Here, we propose a new method to mitigate azimuth streaks based on physical modeling. Azimuth streaks cannot be removed by simply combining the known relationship between ionospheric azimuth offset and the ionospheric phase delay with the phase delay obtained by the split-spectrum method. Thus, taking into account that image matching (coregistration) affects the measurement of azimuth offsets, we formulate a theoretical correction formula of azimuth streaks by subtracting the coregistration-induced effects approximated by a polynomial function from ionospheric azimuth offsets modeled using the split-spectrum method. Applying the method to two pairs of Advanced Land Observing Satellite-2 (ALOS-2)/Phased Array type L-band Synthetic Aperture Radar-2 (PALSAR-2) stripmap images which are severely affected by the ionosphere, we demonstrate effective mitigation of azimuth streaks. In the application to the case that no significant ground movement is detected by Global Navigation Satellite System (GNSS), while the standard deviation of azimuth pixel offset before the correction is 87.2 cm, the value after the correction is 29.2 cm, which is comparable to the theoretical measurement accuracy of the azimuth pixel offset. In the application to the 2016 Kumamoto earthquake, we substantially reduce the azimuth streaks and successfully extract the ground movements from the azimuth offset fields within an accuracy of about 20 cm. The result suggests the proposed method enables more accurate and operational estimation of the 3-D ground displacement.**

***Index Terms*— Advanced Land Observing Satellite-2 (ALOS-2), azimuth streaks estimation, pixel-offset method, split-spectrum method, synthetic aperture radar (SAR).**

## I. Introduction

INTERFEROMETRIC synthetic aperture radar (InSAR) is an essential tool to measure ground movements with an accuracy of a couple of cm. However, the drawbacks are that we can obtain only the 1-D displacement in the line-of-sight (LOS) direction, and it is not available in low coherence areas. In order to complement standard InSAR, methods to measure a displacement in the azimuth direction such as the pixel-offset method [1] and the multiple aperture interferometry (MAI) method [2] have been proposed.

The pixel-offset method using spaceborne synthetic aperture radar (SAR) data has been utilized as a powerful tool to measure large ground movements due to geophysical phenomena [1], [3]–[5]. After conducting image matching (coregistration) between two SAR images, this method is performed by cross-correlating samples of backscatter intensity for each divided patch, and measures the offsets in LOS and azimuth direction (range and azimuth offset, or pixel offsets) of each patch as actual ground movements. By using amplitude instead of phase, the pixel-offset method can robustly measure ground displacements even in low coherence areas where standard InSAR is not available.

The MAI method has been also applied to many large-scale earthquake events to demonstrate its effectiveness [2], [6]. While the MAI method is not applicable in low coherence areas [7], it can enable us to measure ground movements in high coherence areas more accurately than the pixel-offset method [8], [9].

However, the ionosphere can severely affect the low-frequency (e.g., L-band) spaceborne SAR data including MAI and pixel-offset imagery as well as standard InSAR imagery. As a result, ionospheric disturbance can lead to azimuth offsets with streak-like patterns called as "azimuth streaks" in the azimuth direction, and the azimuth streaks often make it difficult to identify the ground displacements in detail [10]–[12]. Therefore, the mitigation of azimuth offset induced by ionospheric disturbance (ionospheric azimuth offset) is one of the major challenges in identifying the ground displacements.

The early studies on the reduction of ionospheric azimuth offset were case studies of Arctic glaciers [13] and the 2008 Sichuan earthquake [11]. They applied a directional filter or a band-cut filter in a frequency domain to pixel-offset imagery, and an interpolation as needed, to successfully extract ground displacements. These techniques can be easily applied to pixel-offset imagery because they do not require physical modeling of ionospheric azimuth offset. However, these techniques are not always suitable because it can result in lowering the accuracy of the offset displacement due to the interpolation [14], or an underestimation of the ground displacement due to the difficulty in separating it from the ionospheric contribution when ground azimuth displacements have the same frequency component as the ionospheric azimuth offset [15].

Over the past decade, remarkable advances have been made in two important theoretical studies on physical modeling of ionospheric azimuth offset. One is the research on the

Manuscript received November 29, 2020; revised February 17, 2021 and March 29, 2021; accepted April 3, 2021. Date of publication April 28, 2021; date of current version December 20, 2021. This work was supported by the Geospatial Information Authority of Japan (GSI). *(Corresponding author: Tatsuya Yamashita.)*

The authors are with the Geospatial Information Authority of Japan, Tsukuba 305-0811, Japan (e-mail: yamashita-t96rq@mlit.go.jp).

This article has supplementary material provided by the authors and color versions of one or more figures available at https://doi.org/10.1109/TGRS.2021.3073511.

Digital Object Identifier 10.1109/TGRS.2021.3073511

relation between azimuth pixel offset and ionospheric phase delay. Gray *et al.* [10] suggested fluctuations in ionospheric electron density may lead to an azimuth shift modulation in SAR imagery. This study led to the formulation of the relationship between ionospheric azimuth offset and ionospheric phase delay [15]–[17]. The other important advance is the development of the split-spectrum method for ionospheric phase screening in InSAR [18]–[21]. This method estimates ionospheric phase delay based on the idea that the SAR imagery is split to generate two subband interferograms with lower and higher center frequencies. Gomba *et al.* [20] was the first work to present an implementation of the method, which enabled the estimation of ionospheric phase delay. As a result of these theoretical advances, ionospheric azimuth offset in MAI imagery was successfully reduced by applying the estimates of ionospheric phase delay obtained by the split-spectrum method to the relationship between ionospheric azimuth offset and ionospheric phase delay [12].

It should be possible in principle to mitigate ionospheric azimuth offset in pixel-offset imagery by following a similar approach to [12]. Therefore, in this article, we first describe the formulation and implementation to estimate ionospheric azimuth offset in pixel-offset imagery. Then the proposed method is validated by two pairs of Advanced Land Observing Satellite-2 (ALOS-2)/Phased Array type L-band Synthetic Aperture Radar-2 (PALSAR-2) stripmap images which are severely affected by ionosphere, for the purpose of investigating the performance of the method.

## II. Theoretical Background

The relationship between ionospheric azimuth offset and the ionospheric phase delay was formulated based on Doppler shift in SAR observations [16], [17]. Based on [16], the following equation can be derived:

$$\Delta x_{\text{iono}} = -\frac{\lambda R_0}{4\pi}\frac{h_{\text{iono}}}{h_{\text{sat}}}\frac{\partial \Delta\phi_{\text{iono}}}{\partial x} \tag{1}$$

where $x$ is the azimuth coordinate, $\Delta x_{\text{iono}}$ is the ionospheric azimuth offset, $R_0$ is the zero Doppler range, $\lambda$ is the microwave wavelength of an SAR satellite sensor, $\Delta\phi_{\text{iono}}$ is the ionospheric phase delay, $h_{\text{sat}}$ is the altitude of the radar satellite, and $h_{\text{iono}}$ is the ionospheric altitude. The derivation of (1) is given in Appendix A. This is a generalization of the formulation by Liang and Fielding [12] in terms of including the dependence on the ionospheric structure as well as the satellite geometry (see Appendix B).

The ionospheric phase delay can be expressed as follows [20]:

$$\Delta\phi_{\text{iono}} = \frac{f_L f_H}{f_0\left(f_H^2 - f_L^2\right)}\left(\Delta\phi_L f_H - \Delta\phi_H f_L\right) \tag{2}$$

where $f_L$ and $f_H$ are the radar center frequencies of the lower and higher subbands, $f_0$ is the center frequency of the original SAR image, and $\Delta\phi_L$ and $\Delta\phi_H$ are differential interferometric phases of the lower and higher spectral subbands. By combining (2) with (1), the formula of ionospheric azimuth offset based on the split-spectrum method can be derived.

It is theoretically expected that the ionospheric azimuth offset in pixel-offset imagery can be removed by using $\Delta x_{\text{iono}}$ estimated by the split-spectrum method. However, as demonstrated in Section V-A, the azimuth streaks simply cannot be removed by the theoretically derived ionospheric azimuth offsets based on (1) and (2). Here, we should note that in most cases two radar images are coregistered to obtain pixel offsets based on a low-order polynomial function such as an affine transformation and uniform shift. Thus it seems likely that coregistration will affect the estimates of azimuth offsets. Here, we derive a theoretical correction formula of ionospheric azimuth offset based on the following assumptions.

1) Azimuth offset before coregistration, $\Delta x_{\text{bc}}$, consists of the offset due to the difference of position and orientation of the spaceborne SAR sensor, $\Delta x_{\text{geom}}$, the component of ground movements, $\Delta x_{\text{defo}}$, the ionospheric azimuth offset, $\Delta x_{\text{iono}}$, and the noise associated with the other phenomena, $\Delta x_{\text{others}}$.
2) $\Delta x_{\text{others}}$ is negligible compared to $\Delta x_{\text{geom}}$, $\Delta x_{\text{defo}}$, and $\Delta x_{\text{iono}}$.
3) While a part of $\Delta x_{\text{iono}}$ is removed by coregistration, $\Delta x_{\text{defo}}$ is completely preserved, even after the coregistration, by selecting image tie-points in the area where $\Delta x_{\text{defo}}$ is expected to be nearly zero.
4) Coregistration is conducted accurately enough to consider the estimation error of $\Delta x_{\text{geom}}$, $\varepsilon_{\text{geom}}$, as being negligible compared to the other components.
5) Ionospheric phase delay obtained by the split-spectrum method, $\Delta\phi_{\text{iono}}^{\text{SS}}$, consists of a systematic part that is removed by coregistration ($\Delta\phi_{\text{iono}}^{c}$), a residual part independent of coregistration ($\Delta\phi_{\text{iono}}^{\text{nc}}$), and high-frequency random noise $\varepsilon_{\text{noise}}$, where the expectations of $\Delta\phi_{\text{iono}}^{\text{nc}}$and$\varepsilon_{\text{noise}}$ are approximately zero.
6) $\varepsilon_{\text{noise}}$ can be removed by applying a low-pass filter.

We first formulate the azimuth offset before and after coregistration. Based on assumption 1), the azimuth offset before coregistration, $\Delta x_{\text{bc}}$, is expressed as

$$\Delta x_{\text{bc}} = \Delta x_{\text{geom}} + \Delta x_{\text{defo}} + \Delta x_{\text{iono}} + \Delta x_{\text{others}}. \tag{3}$$

By assumption 2), (3) can be approximated as

$$\Delta x_{\text{bc}} \approx \Delta x_{\text{geom}} + \Delta x_{\text{defo}} + \Delta x_{\text{iono}}. \tag{4}$$

Further by assumption 3), we obtain

$$\Delta x_{\text{iono}} = \Delta x_{\text{iono}}^{c} + \Delta x_{\text{iono}}^{\text{nc}} \tag{5}$$

where $\Delta x_{\text{iono}}^{c}$ denotes the ionospheric azimuth offset that can be removed by coregistration, and $\Delta x_{\text{iono}}^{\text{nc}}$ is the nonremovable component. Substituting (5) into (4)

$$\Delta x_{\text{bc}} \approx \Delta x_{\text{geom}} + \Delta x_{\text{defo}} + \Delta x_{\text{iono}}^{\text{c}} + \Delta x_{\text{iono}}^{\text{nc}}. \tag{6}$$

In (6), note that $\Delta x_{\text{geom}}$ and $\Delta x_{\text{iono}}^{c}$ can be removed by coregistration. Therefore, if the azimuth offset after coregistration is denoted by $\Delta x_{\text{ac}}$, then by assumption 4)

$$\Delta x_{\text{ac}} \approx \Delta x_{\text{defo}} + \Delta x_{\text{iono}}^{\text{nc}} + \varepsilon_{\text{geom}} \approx \Delta x_{\text{defo}} + \Delta x_{\text{iono}}^{\text{nc}} \tag{7}$$

where $\Delta x_{\text{ac}}$ corresponds to an azimuth offset obtained by standard pixel-offset analysis, and $\Delta x_{\text{iono}}^{\text{nc}}$ is the component corresponding to azimuth streaks. The problem in detecting the ground movement contribution $\Delta x_{\text{defo}}$ is how we separate

$\Delta x_{\text{iono}}^{\text{nc}}$ from the ground movement contribution to extract it. Thus, we next focus on the formulation of the separation and extraction of $\Delta x_{\text{iono}}^{\text{nc}}$. If ionospheric phase delay components corresponding to $\Delta x_{\text{iono}}^{c}$ and $\Delta x_{\text{iono}}^{\text{nc}}$ are denoted by $\Delta\phi_{\text{iono}}^{c}$ and $\Delta\phi_{\text{iono}}^{\text{nc}}$, respectively, then

$$\Delta x_{\text{iono}}^{c} = -\frac{\lambda R_0}{4\pi}\frac{h_{\text{iono}}}{h_{\text{sat}}}\frac{\partial \Delta\phi_{\text{iono}}^{c}}{\partial x} \tag{8}$$

and

$$\Delta x_{\text{iono}}^{\text{nc}} = -\frac{\lambda R_0}{4\pi}\frac{h_{\text{iono}}}{h_{\text{sat}}}\frac{\partial \Delta\phi_{\text{iono}}^{\text{nc}}}{\partial x}. \tag{9}$$

Furthermore, by assumption 5), $\Delta\phi_{\text{iono}}^{\text{SS}}$ is expressed as

$$\Delta\phi_{\text{iono}}^{\text{SS}} = \Delta\phi_{\text{iono}}^{c} + \Delta\phi_{\text{iono}}^{\text{nc}} + \varepsilon_{\text{noise}} \tag{10}$$

where since the expectations of $\left|\Delta\phi_{\text{iono}}^{\text{nc}}\right|$ and $|\varepsilon_{\text{noise}}|$ are approximately zero, we can obtain unbiased estimates of $\Delta\phi_{\text{iono}}^{c}$ through the approximation of $\Delta\phi_{\text{iono}}^{\text{SS}}$ by the polynomial that satisfies (8). Thus, if we derive a polynomial approximation of $\Delta\phi_{\text{iono}}^{\text{SS}}$, which is denoted by $\left[\Delta\phi_{\text{iono}}^{\text{SS}}\right]^{\text{poly}}$, then we obtain

$$\left[\Delta\phi_{\text{iono}}^{\text{SS}}\right]^{\text{poly}} \approx \Delta\phi_{\text{iono}}^{c}. \tag{11}$$

Subtracting (10) from (11), we obtain the following approximate expression:

$$\Delta\phi_{\text{iono}}^{\text{SS}} - \left[\Delta\phi_{\text{iono}}^{\text{SS}}\right]^{\text{poly}} \approx \Delta\phi_{\text{iono}}^{\text{nc}} + \varepsilon_{\text{noise}}. \tag{12}$$

If the overbar denotes low-pass filter processing, then by assumption 6), we obtain

$$\overline{\Delta\phi_{\text{iono}}^{\text{SS}} - \left[\Delta\phi_{\text{iono}}^{\text{SS}}\right]^{\text{poly}}} \approx \Delta\phi_{\text{iono}}^{\text{nc}}. \tag{13}$$

By combining (7), (9), and (13), we finally find that

$$\Delta x_{\text{defo}} \approx \Delta x_{\text{ac}} + \frac{\lambda R_0}{4\pi}\frac{h_{\text{iono}}}{h_{\text{sat}}}\frac{\partial}{\partial x}\left[\overline{\Delta\phi_{\text{iono}}^{\text{SS}} - \left[\Delta\phi_{\text{iono}}^{\text{SS}}\right]^{\text{poly}}}\right]. \tag{14}$$

Equation (13) indicates that we can estimate ionospheric azimuth offset by applying polynomial approximation to the ionospheric phase delay obtained by the split-spectrum method, and employing a spatial filter for the residuals. In addition, as (14) indicates, we are able to separate, approximately, ionospheric azimuth offset from the ground movement contribution after correcting ionospheric azimuth offset making use of (13).

## III. Implementation

In this section, we describe an example of the implementation for correcting ionospheric azimuth offset. In this study, we used GSISAR software [22]–[25] for interferometric processing including the split-spectrum method, and GAMMA-SAR software [26] to generate pixel-offset imagery. The processing flowchart is presented in Fig. 1, and the detail of the processing is described below. First, in order to obtain the azimuth pixel offset, a standard pixel-offset method was applied to two single look complex (SLC) images. Specifically, the method included an elevation-dependent correction [11], a subpixel coregistration of SLC images [23], pixel offset estimation, and median filtering. In this study, we used a program of GAMMA-SAR software, "offset_pwr_tracking" [27] to adopt incoherent patch-based shift estimation.

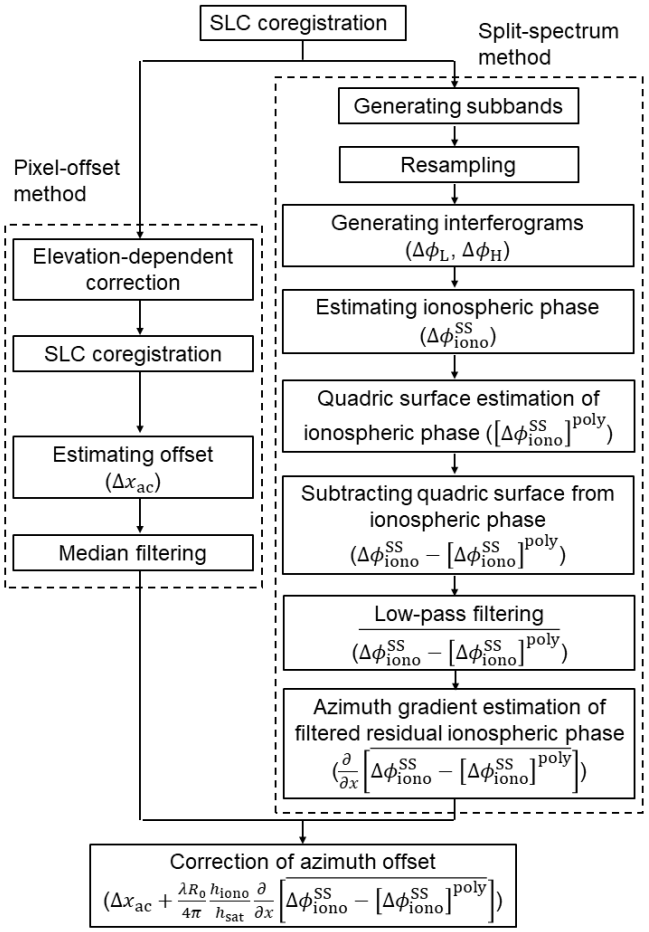


Fig. 1. Flowchart of the implementation for correcting the ionospheric azimuth offset.

After the application of a standard pixel-offset method, the ionospheric phase delay $\Delta\phi_{\text{iono}}^{\text{SS}}$ is obtained based on the split-spectrum method. To increase the robustness of the estimation, the refinement proposed by Wegmüller *et al.* [21] is applied, in which split-spectrum double difference phase and full-bandwidth interferogram are used instead of upper and lower spectral subband interferograms to make unwrapping easier.

Second, the polynomial approximation for the ionospheric phase delay $\left[\Delta\phi_{\text{iono}}^{\text{SS}}\right]^{\text{poly}}$ is estimated. Here we employed an affine transformation, thus from (8), $\left[\Delta\phi_{\text{iono}}^{\text{SS}}\right]^{\text{poly}}$ takes the form of a quadric surface. In this study, a weighted least squares method is applied to obtain the estimates, and the weight coefficients are given by the inverse-square of the theoretical standard deviation of the ionospheric phase delay [20].

Next, the estimate of $\Delta\phi_{\text{iono}}^{\text{nc}}$ can be obtained by subtracting the approximate quadric surface $\left[\Delta\phi_{\text{iono}}^{\text{SS}}\right]^{\text{poly}}$ from the ionospheric phase delay $\Delta\phi_{\text{iono}}^{\text{SS}}$.

The low-pass filter is applied to the residuals to suppress high frequency noise which can have a negative influence on an evaluation of the azimuth gradient of the ionospheric phase

TABLE I
INFORMATION ON THE ALOS-2/PALSAR-2 IMAGE DATA USED IN THE CASE STUDIES

| Case | Track | Frame | First Observation | Second Observation | Mode | Direction |
|---|---|---|---|---|---|---|
| Hokkaido | 122 | 850 | 06/06/2015 | 04/06/2016 | SM1 | AR |
| Kumamoto | 29 | 2910, 2920 | 14/01/2015 | 20/04/2016 | SM1 | DL |

delay. In this study, we adopted a 2-D weighted Gaussian filter. When applying a Gaussian filter, care is required when choosing the appropriate standard deviation of the filter just as the other approaches proposed to mitigate ionospheric effects on InSAR and pixel-offset methods: if the standard deviation is larger than the dominant spatial scale of the azimuth streaks, the signal component of the ionospheric phase delay can be too smoothed to evaluate appropriately. In this study, we examined the optimal standard deviation of the filter to find the best result in terms of the statistics on the residuals for all the pixels in the area with little ground movement. Since the object function to be optimized is the nonlinear function of the standard deviation of the filter, we applied the grid search method to the standard deviation of the filter, and adopted 1 km as the incremental value. This procedure enables objective determination of the optimal standard deviations which might otherwise require experiences of the SAR operators.

Subsequently, the azimuth gradient of the filtered residuals is calculated. In this study, the gradient is evaluated by applying a second-order centered difference scheme. Empirically, if high frequency noise is removed appropriately by the low-pass filter, the azimuth gradient of the filtered residuals can be evaluated accurately using a simple second-order centered difference scheme.

Finally, the correction amount is evaluated using the estimated azimuth gradient to be subtracted from the azimuth pixel offset. Here, we applied the linear least squares calculation to determine an optimal value of ionospheric altitude $h_{\mathrm{iono}}$ for mitigation of ionospheric azimuth offset for each standard deviation of the Gaussian filter, and adopted the result with the best measurement accuracy. For estimating $h_{\mathrm{iono}}$ properly, we assumed the azimuth offset can include not only ionospheric azimuth offset but also the uniform bias. Furthermore, we considered the obtained solutions as invalid if $h_{\mathrm{iono}}$ was within the possible range (250–450 km), considering that the ionospheric altitude is fixed to be a constant value within 350–450 km in most conventional ionospheric models for Global Navigation Satellite System (GNSS) positioning [28], and that estimation approaches of the ionospheric altitude based on azimuth subband shifts [29] and Faraday rotation of microwave signals [16] were proposed in recent years, estimating the ionospheric altitude at 250–280 km.

## IV. CASE STUDIES ON MITIGATING IONOSPHERIC AZIMUTH OFFSET

In this section, we apply the correction method of ionospheric azimuth offset described in Sections II and III to two pairs of ALOS-2/PALSAR-2 images over Japan, in which substantial ionospheric azimuth offset can be found (Table I), to investigate the performance of ionospheric azimuth offset mitigation. In the first case (Hokkaido), we selected an area with little ground movement as our research target; and in the second case (Kumamoto), we focused on an area with large ground movements due to the 2016 Kumamoto earthquake. The objective of the case study in Hokkaido area is to examine how much the ionosphere-induced noise can be reduced. On the other hand, the objective of the case study in the Kumamoto area is to examine how accurately the ground movements can be extracted by correcting for ionospheric azimuth offset.

In the least squares calculation to determine $h_{\mathrm{iono}}$ for the case of Hokkaido area, we adopted all available pixels on the land area. On the other hand, in the case of Kumamoto area, we show the result of the least squares estimation excluding the pixels with ground motion of more than 10 cm in order to see the best performance. The case of Kumamoto area using all available pixels is described in Section V.

### A. Hokkaido

In the case study of Hokkaido, significant ionospheric phase delay was detected in InSAR imagery despite little ground movement at GNSS Continuously Operating Reference Stations (CORS) (Table S1). However, after applying the split-spectrum method, there were no significant fringes in the InSAR imagery, which implies that we successfully estimate ionospheric phase delay $\Delta\phi_{\mathrm{iono}}^{\mathrm{SS}}$ (Fig. S1). Correspondingly, significant periodic azimuth streaks emerge in azimuth pixel offsets obtained by the pixel-offset method [Fig. 2(a)]. The correction amount of ionospheric azimuth offset has a spatial structure in common with the azimuth pixel offset [Fig. 2(b)], and having nearly the same amplitude in most areas, as well as the same sign. Accordingly, a large part of ionospheric azimuth offset is canceled out by applying the correction to the azimuth pixel offset obtained by the pixel-offset method [Fig. 2(c)]. Focusing on the statistics, while the standard deviation of the offset before the correction was 87.2 cm, the value after the correction was 29.2 cm, indicating that the ionospheric azimuth offset can be considerably compensated through the correction. Especially, it is noteworthy that the standard deviation after the correction is comparable to the theoretical measurement accuracy of the azimuth pixel offset method, 30 cm [8]. In addition, while the mean value of the offset for all the pixels before the correction was $-3.8$ cm, the value after the correction was $-6.9$ cm, which indicates no significant artificial biases were added by the correction.

In this case study, the best measurement accuracy was achieved when the standard deviation for the Gaussian filter was 6 km, and the optimum value of $h_{\mathrm{iono}}$ was 403.5 km (Fig. S2). When the standard deviation for the filter was 6 km, there was no high frequency noise or excessive smoothing observed in the imagery (Fig. S3).

### B. Kumamoto

Various studies on the ground movements due to the 2016 Kumamoto earthquakes have been reported, and

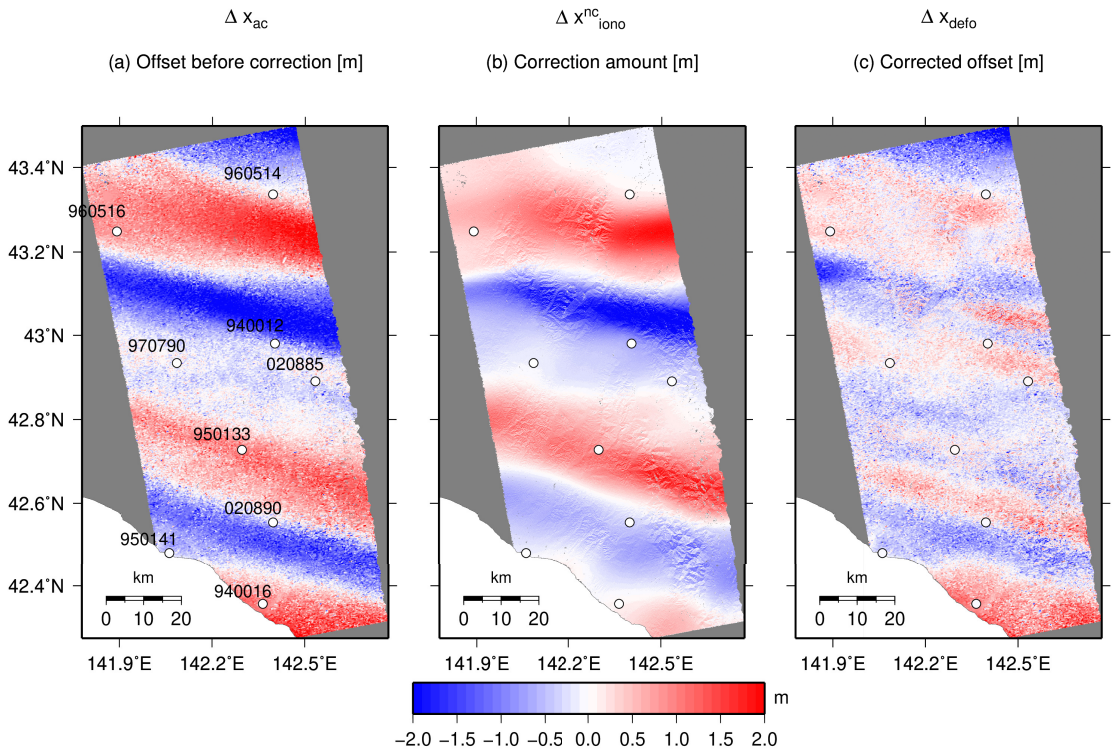


Fig. 2. Correction of the ionospheric azimuth offset in the case study of Hokkaido area. (a) Azimuth pixel offset before the correction. The standard deviation of the offset was 87.2 cm, and the mean value of the offset for all pixels was −3.8 cm. (b) Correction amount calculated using (9) and (13). (c) Azimuth pixel offset after the correction [(a) and (b)]. The standard deviation of the offset was 29.2 cm, and the mean value of the offset for all pixels after the correction was −6.9 cm. Circles show the location of GNSS CORS, and the azimuth offsets converted from GNSS CORS displacements are also shown at the points.

the whole picture of the movements is being clarified [4], [30]–[32]. While coseismic ground movements exceeding 2 m in both horizontal and vertical direction were observed near the main source faults (black lines in Fig. 3), the displacement at GNSS CORS located in the far-field (>30–40 km distant from the faults) was less than 10 cm [Fig. 3(a)].

In InSAR imagery used in the case study of Kumamoto, significant ionospheric phase delay was detected in the far-field of the 2016 Kumamoto earthquakes. After an application of the split-spectrum method, there were no significant fringes in the far-field, which implies that we successfully estimated $\Delta\phi^{\mathrm{SS}}_{\mathrm{iono}}$ (Fig. S4). Correspondingly, we found azimuth pixel offsets of approximately 1 m in the far-field area [Fig. 3(a)], which implied the presence of an ionospheric azimuth offset. The estimated correction amount $\Delta x^{\mathrm{nc}}_{\mathrm{iono}}$ revealed a similar pattern to the azimuth offset obtained by standard pixel-offset method [Fig. 3(a) and (b)]. Actually, after an application of the correction, the major part of azimuth offset in the far-field was removed [Fig. 3(c)].

We next evaluated quantitatively the accuracy of the correction of ionospheric azimuth offset. In contrast to the case study in Hokkaido area, the image used in this case study includes significant ground movements near the main faults (black lines in Fig. 3). Therefore, we evaluated not only the standard deviation and mean value of the corrected azimuth pixel offset for all the pixels at which the magnitude of ground movements was expected to be less than about 10 cm, but also the residuals between the azimuth offset converted from GNSS CORS displacement and the offset based on pixel-offset method.

In the area with little ground movement (<10 cm), while the standard deviation of the offset before the correction was 15.5 cm, the value after the correction was 10.7 cm. In addition, while the mean value before the correction was 0.1 cm, the value after the correction was 0.0 cm. These results indicate the improvement of measurement accuracy in the far-field of the 2016 Kumamoto earthquake.

After applying the correction, the residuals between the azimuth offsets converted from GNSS CORS displacements and the offsets based on the pixel-offset method were improved at 19 out of 27 GNSS CORS in the scene covering the Kumamoto area (CORS ID displayed in magenta in Fig. 4). It is especially notable that the residuals were improved at the CORS near the main source faults (e.g., 021 071, 950 465, and 960 701). While the maximum residual before the correction was approximately 70.0 cm, the residuals after the correction were less than about 33.5 cm at all the CORS. As for the statistics, the standard deviations of the residuals before and after the correction were 37.4 and 18.8 cm, respectively: the deviation gets smaller through the correction. Moreover, the mean values of the residuals before and after the correction were −7.8 and −6.9 cm, respectively. Although the negative systematic bias still exists after the correction, the value gets smaller. These results suggest that the ground movement in the azimuth direction can be extracted within an accuracy of about 20 cm by correcting for the ionospheric azimuth offset.

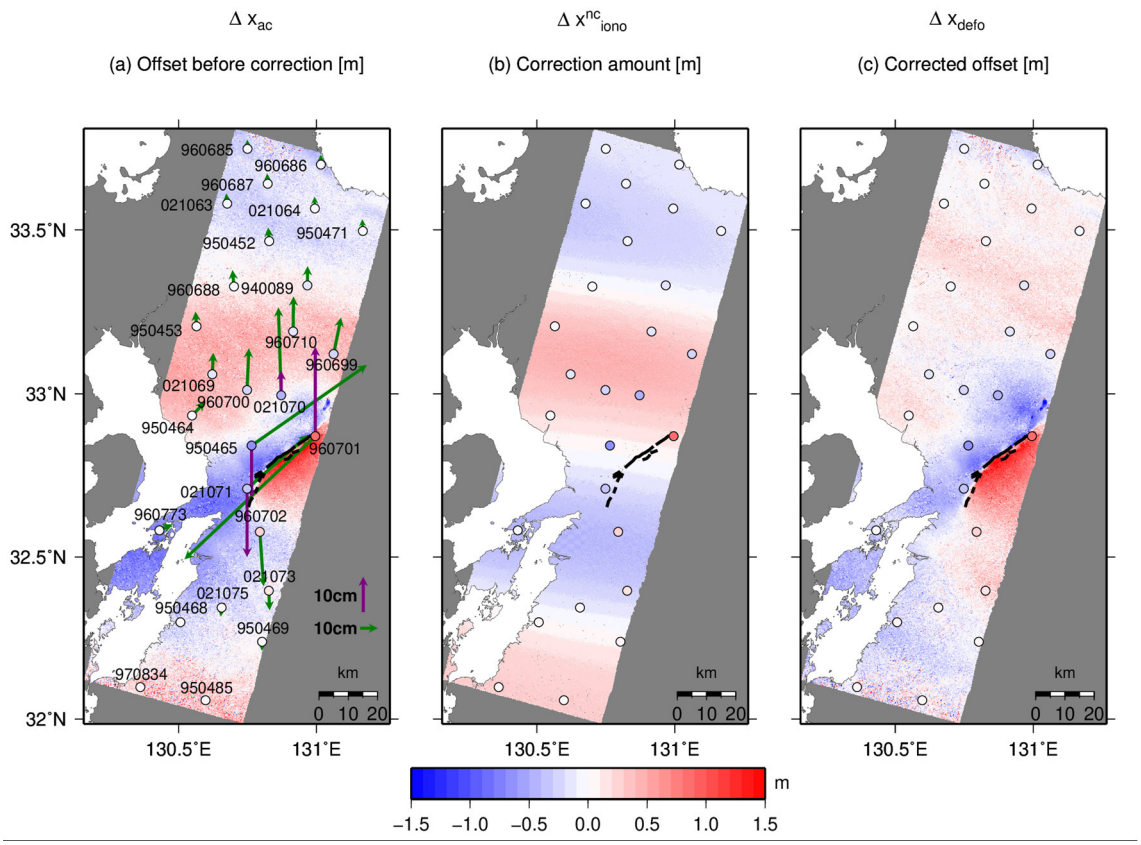


Fig. 3. Same as Fig. 2 but for Kumamoto area with different color range, horizontal (green arrows) and vertical (magenta arrows) component of displacement at GNSS CORS, and traces of active faults published by the Headquarters for Earthquake Research Promotion in Japan (black lines).

In the case study of the Kumamoto area, the best measurement accuracy in the area with little ground movement was achieved when the standard deviation for the Gaussian filter was 22 km, and the optimum value of $h_{\text{iono}}$ was 445.6 km (Fig. S5). When the standard deviation for the filter was 22 km, there was no high frequency noise or excessive smoothing observed in the imagery (Fig. S6).

## V. Discussion

### *A. Importance of Considering Partial Elimination of the Ionospheric Azimuth Offset by Coregistration*

In this section, we demonstrate that the ionospheric azimuth offset cannot be reduced by simply combining the relationship between ionospheric azimuth offset and the ionospheric phase delay (1) and the equation of ionospheric phase delay (2) without considering the partial elimination of the ionospheric azimuth offset through coregistration. Fig. 5 shows the result in the case where the approximate quadric surface is not subtracted from the ionospheric phase delay obtained by the split-spectrum method. Unlike Fig. 2, there were not any periodic patterns seen in the ionospheric azimuth offset. The correction value was larger than that of Fig. 2, and consequently significant negative biases were added in most of the area after applying the correction to the azimuth pixel offset. Focusing on the statistics, the mean value and the standard deviation of the offset after the correction were −143.1 and 238.6 cm, respectively, thus the values after the correction were larger than the uncorrected values. The degradation of the mean value and the standard deviation after the correction could also be observed in the case study in the Kumamoto area. These results indicate it is essential to subtract the component associated with the coregistration from the ionospheric phase delay obtained by the split-spectrum method, considering the partial elimination of the ionospheric azimuth offset achieved through the coregistration.

### *B. Remaining Bias After the Correction and the Possibility of the Refinement*

In Section IV, while we effectively mitigated the azimuth streaks to an accuracy of 20–30 cm, we also noted the remaining bias after the correction in both cases, which was not explainable on the basis of the formulation proposed in Section II. This bias could possibly be generated by filtering in low coherence areas, as Gomba *et al.* [20] and Liang and Fielding [12] pointed out. The other possibility is that the bias could result from the elevation-dependent correction in the pixel-offset method, that is, the difference of coregistration data between the pixel-offset method and the split-spectrum method. Although the fundamental solution should be further investigated as future work, we made an *ad hoc* correction of the bias focusing on the refinement of the case study of Hokkaido.

In Section IV, while we assumed the azimuth offset included the uniform bias for the proper least squares estimation of

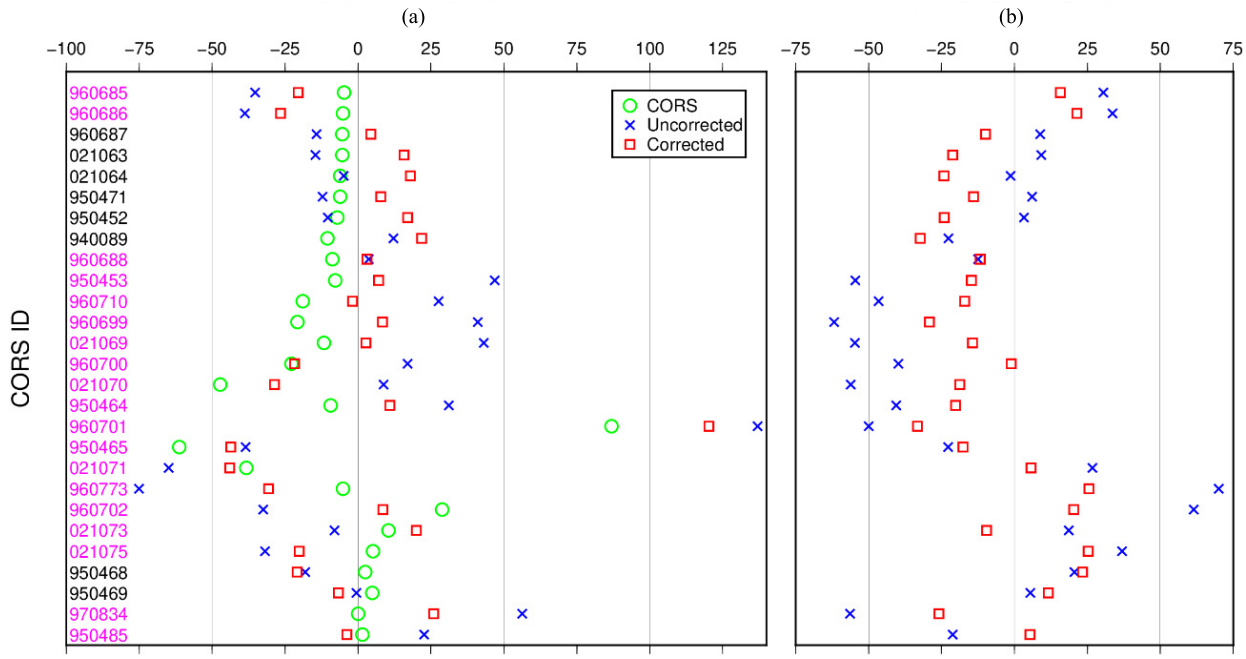


Fig. 4. Azimuth offsets at GNSS CORS in the case study of the Kumamoto area. (a) Azimuth offset converted from GNSS CORS displacement (green circles), the azimuth offset before the correction (blue crosses), and that after the correction (red squares). (b) Residuals of the azimuth offset before the correction (blue crosses) and that after the correction (red squares). ID of GNSS CORS at which the residuals were improved are displayed in magenta. We adopted the station 970 834 as the reference station, and calculated the CORS displacement by subtracting the mean value within five days of the master observation date from that of the master observation date. The standard deviation of the residuals before and after the correction was 37.4 and 18.8 cm, respectively. The mean values of the residuals before and after the correction were −7.8 and −6.9 cm, respectively.

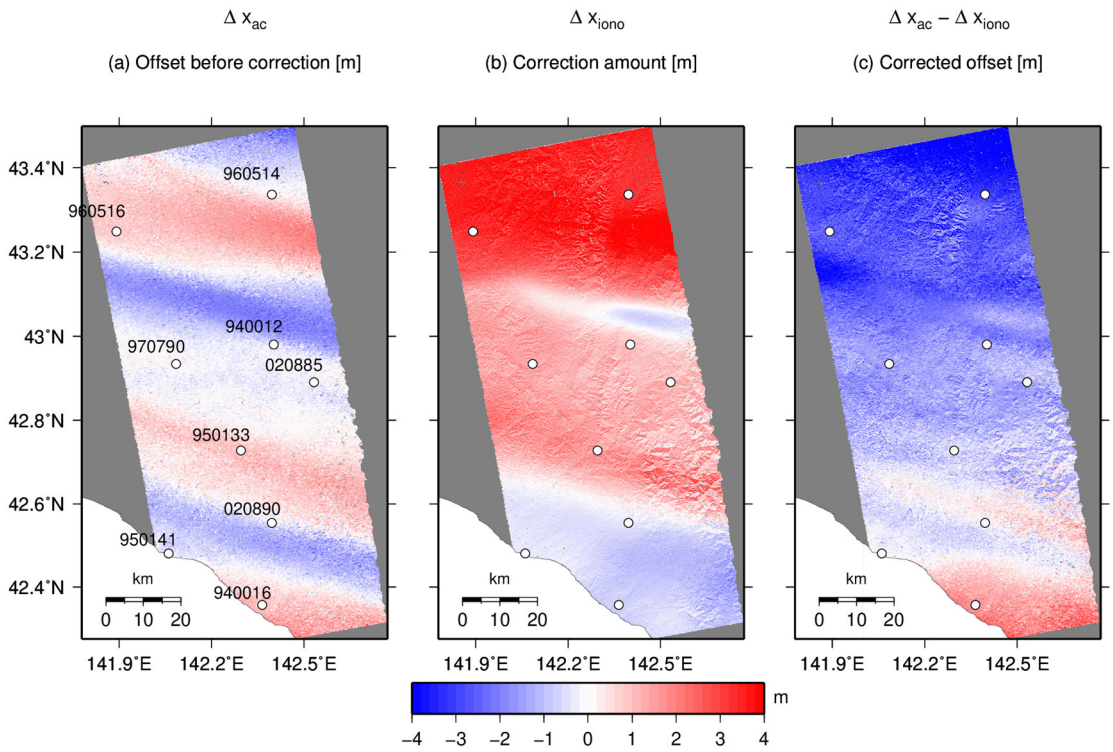


Fig. 5. Correction of the ionospheric azimuth offset without subtracting the quadric surface from ionospheric phase delay in the case study of Hokkaido area. The standard deviation of the offset was 238.6 cm, and the mean value of the offset for all pixels after the correction was −143.1 cm. Note that the color range is different from that of Fig. 2.

$h_{\mathrm{iono}}$, we did not subtract the bias when evaluating the statistics. After the correction and subtracting the bias, the mean value and the standard deviation of the offset for all the pixels available were 0.1 and 29.2 cm, respectively. Although the bias was considerably decreased, the standard deviation was not improved. Aiming to improve the measurement accuracy,

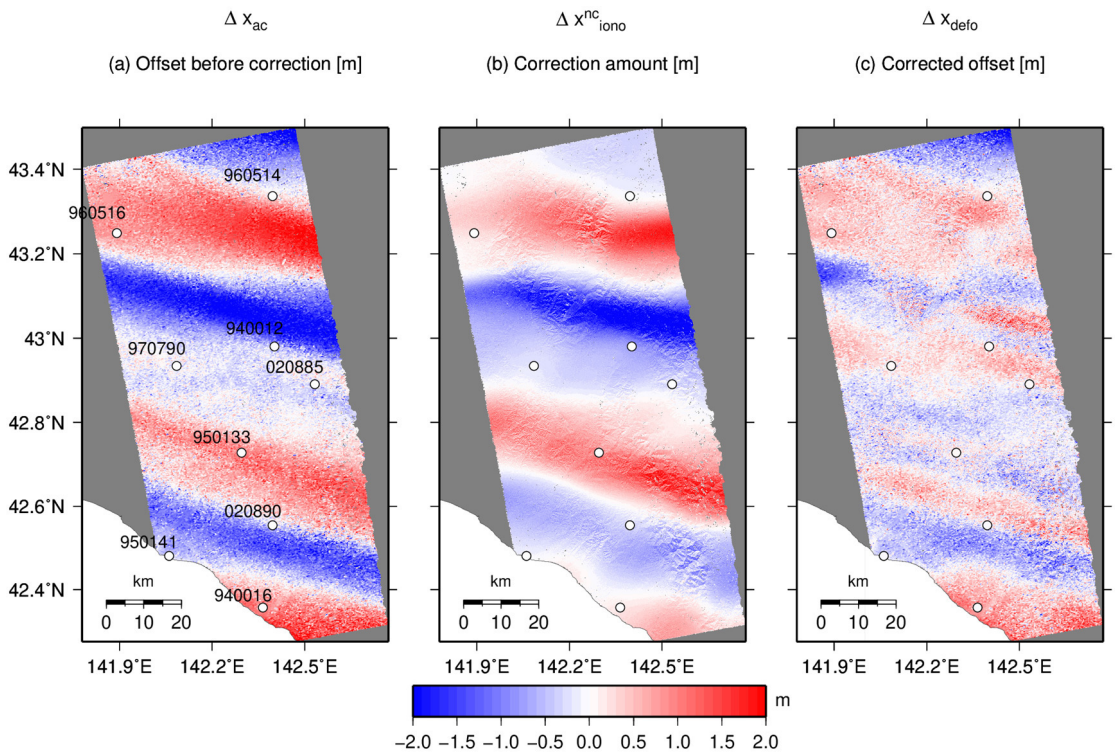


Fig. 6. Same as Fig. 2 but for $h_{\text{iono}} = 409.6$ km and subtracting the bias fitted by a linear plane. The standard deviation of the offset was 28.2 cm, and the mean value of the offset for all pixels after the correction was −0.1 cm.

we next assumed the remaining ramp in Fig. 2(c), and estimated the bias based on planar approximation. In this case, the optimum value of $h_{\text{iono}}$ was 409.6 km, and the residuals got smaller in the northernmost and southernmost area (Fig. 6). As for the statistics, the mean value was still 0.1 cm, and the standard deviation was decreased to 28.2 cm.

The correction on the basis of planar approximation did not improve the mean and standard deviation of the offset in the case study of Kumamoto, possibly due to the existence of the ground movement. Thus we conclude the linear least squares method under the assumption of a planar bias is not universal, but *ad hoc* at this moment.

### C. Sensitivity of the Least Square Estimation to the Presence of Ground Motion

In order to see the sensitivity of the least square estimation to the presence of ground motion, we tested the case of Kumamoto area using all available pixels, as well as the case excluding the pixels at which the magnitude of ground movements was expected to be more than about 10 cm based on GNSS CORS and InSAR imagery. In the case using all available pixels, the standard deviation of the residuals at GNSS CORS after the correction was 20.6 cm. Although it was slightly larger than the standard deviation when excluded the pixels with ground motion of more than 10 cm, the ground movement in the azimuth direction can be still extracted within an accuracy of about 20 cm by the correction. This indicates the least square estimation is not sensitive to the ground motion. This insensitivity would be related to the empirical fact that ground motions due to geophysical phenomena do not have a streak-like pattern.

## VI. Conclusion

In this article, we presented the formulation and implementation of mitigation of ionospheric noise in azimuth pixel offsets on the basis of the relationship between the ionospheric azimuth offset and ionospheric phase delay in an InSAR image, and the split-spectrum method. In addition, we applied the proposed correction method to two pairs of ALOS-2/PALSAR-2 images over Japan which are severely affected by the ionosphere. In the case study of the Hokkaido area, in which there is little ground movement (Section IV-A), the standard deviation of azimuth pixel offsets after the correction was comparable to the theoretical measurement accuracy (30 cm). And in the case study of Kumamoto area in which large ground movements were induced by the 2016 Kumamoto earthquake (Section IV-B), we demonstrated ground movement contribution to the azimuth pixel offset could be extracted with an accuracy of about 20 cm. These results indicate that the measurement accuracy of corrected data is expected to be comparable to that of data which are not affected by ionospheric disturbance.

Because the proposed correction approach is based on physical modeling, it enables SAR operators to separate a ground motion from azimuth streaks without underestimation of the ground motion. As a result, they get to fully use the pixel-offset data corrupted by ionospheric disturbance after correction. This is of great importance in accurate estimation of 3-D displacement field due to geophysical phenomena using

combined geodetic data, because pixel-offset method complements InSAR in terms of obtaining along-track displacement especially in low coherence area.

A major drawback of the proposed correction method is that we have to evaluate the ionospheric azimuth offset by extrapolation in the decorrelated area of the InSAR image due to calculating the ionospheric phase delay based on the split-spectrum method. If the decorrelation spreads out over a large area, we must expect the degradation of the estimation accuracy in the central part of the area. One option for improving the accuracy in an extensive decorrelation area would be through the application of GNSS CORS data in the area to the correction, which is left as a further investigation. The other drawback is the potential degradation of the estimation accuracy if using lower resolution modes [i.e., SM2, SM3, and wide area observation mode (WD)] of ALOS-2/PALSAR-2 image, since the measurement accuracy of ionospheric phase delay based on the split-spectrum method is inversely proportional to bandwidth [20], [25]. The bandwidth of SM1 is 84 MHz, those of SM2 and SM3 are 42 and 28 MHz, respectively, and that of WD is 14 or 28 MHz. Therefore, the measurement accuracy for these other modes is expected to be more than twice as bad as that of SM1. However, an upcoming L-band spaceborne SAR satellite, ALOS-4, will provide a split-band observation mode (28 + 10 MHz) to correct ionospheric phase delay more precisely in InSAR analysis [33], which will solve the problem of degradation of the estimation accuracy using the lower resolution modes. Moreover, ALOS-4 will conduct observations more frequently, and improve the measurement accuracy of the split-spectrum method. This is because the measurement accuracy of the split-spectrum method gets better with the interferometric coherence [20], and more frequent observation tends to increase the interferometric coherence. The quantitative investigations are left as work after the onset of the operation of ALOS-4.

## Appendix A Derivation of (1)

Here we derive (1) by combining several equations shown in [16]. From (5.71) in [16], the ionospheric azimuth offset of a single image (in pixels) is given by

$$\Delta a = 2\zeta \frac{v_{\text{piercing}}}{\text{cf}_0} \frac{\text{PRF}}{D_R} \frac{\partial \text{TEC}}{\partial x} \tag{15}$$

where $\zeta = 40.28$ [m$^3$/s$^2$], $v_{\text{piercing}}$ is the velocity of the ionospheric piercing point of LOS, $c$ is the speed of light, $f_0$ is the center frequency, PRF is the pulse repetition frequency, $D_R$ is the Doppler rate, and TEC is the total electron content. If satellite speed and ionospheric azimuth offset of a single image (in length) are denoted by $v_{\text{sat}}$ and $\Delta\hat{a}$, respectively, multiplying both sides of (15) by $v_{\text{sat}}$/PRF, we find

$$\Delta\hat{a} = 2\zeta \frac{v_{\text{piercing}}}{\text{cf}_0} \frac{v_{\text{sat}}}{D_R} \frac{\partial \text{TEC}}{\partial x}. \tag{16}$$

If the differential azimuth offset between the first and second observation is denoted by $\Delta x_{\text{iono}}$, we obtain the following relationship from (16):

$$\Delta x_{\text{iono}} = 2\zeta \frac{v_{\text{piercing}}}{\text{cf}_0} \frac{v_{\text{sat}}}{D_R} \frac{\partial \Delta\text{TEC}}{\partial x} \tag{17}$$

where $\Delta$TEC is the differential TEC between two images. From (5.67) in [16]

$$\frac{2v_{\text{sat}}^2}{cR_0} = \frac{D_R}{f_0} \tag{18}$$

where $R_0$ is the zero Doppler range. Combining (17) and (18) to eliminate $D_R$

$$\Delta x_{\text{iono}} = \frac{\zeta v_{\text{piercing}} R_0}{v_{\text{sat}} f_0^2} \frac{\partial \Delta\text{TEC}}{\partial x}. \tag{19}$$

Using the relationship between $v_{\text{piercing}}$ and $v_{\text{sat}}$ shown in p.109 of [16]

$$v_{\text{piercing}} = v_{\text{sat}} \frac{h_{\text{iono}}}{h_{\text{sat}}} \tag{20}$$

we can eliminate $v_{\text{piercing}}$ in (19)

$$\Delta x_{\text{iono}} = \frac{\zeta R_0}{f_0^2} \frac{h_{\text{iono}}}{h_{\text{sat}}} \frac{\partial \Delta\text{TEC}}{\partial x}. \tag{21}$$

Moreover from (5.57) in [16]

$$\Delta\phi_{\text{iono}} = -\frac{4\pi\zeta}{\text{cf}_0}\Delta\text{TEC} = -\frac{4\pi\zeta}{f_0^2\lambda}\Delta\text{TEC} \tag{22}$$

where $\lambda$ is the microwave wavelength of an SAR satellite sensor. By combining (21) and (22) to eliminate $\Delta$TEC, we finally obtain (1)

$$\Delta x_{\text{iono}} = -\frac{\lambda R_0}{4\pi} \frac{h_{\text{iono}}}{h_{\text{sat}}} \frac{\partial \Delta\phi_{\text{iono}}}{\partial x}. \tag{23}$$

## Appendix B Difference in Formulations Between [12] and [16]

In this section, we first derive the relation between ionospheric azimuth offset and the ionospheric phase delay on the basis of [12]. From (6) in [12]

$$\Delta x_{\text{iono}} = -\frac{\Delta\phi_{\text{MAI}} v_g}{2\pi\left(f_{\text{dc},f} - f_{\text{dc},b}\right)} \tag{24}$$

where $\Delta\phi_{\text{MAI}}$ is the phase of MAI imagery, $v_g$ is the velocity of the beam footprint on the ground, $f_{\text{dc},f}$ and $f_{\text{dc},b}$ are the Doppler centroid frequencies of forward and backward looks, respectively. From (15) in [12], the phase of MAI imagery is given by

$$\Delta\phi_{\text{MAI}} = \frac{nT_c}{2} \frac{\partial \Delta\phi_{\text{iono}}}{\partial \eta} \tag{25}$$

where $n$ is the difference of burst numbers, $T_c$ is burst cycle length, and $\eta$ is azimuth time. And note that the sign of right-hand side of (25) is different from the original equation in [12] because the differential ionospheric phase delay in [12] is defined to have the opposite sign to that in [16]. Combining (24) and (25) to eliminate $\Delta\phi_{\text{MAI}}$, we obtain

$$\Delta x_{\text{iono}} = -\frac{v_g n T_c}{4\pi\left(f_{\text{dc},f} - f_{\text{dc},b}\right)} \frac{\partial \Delta\phi_{\text{iono}}}{\partial \eta}. \tag{26}$$

From (3) in [12]

$$f_{\text{dc},f} = \frac{2v_{\text{sat}} \sin\theta_{\text{sq},f}}{\lambda} \tag{27}$$

and

$$f_{\mathrm{dc},b} = \frac{2v_{\mathrm{sat}} \sin\theta_{\mathrm{sq},b}}{\lambda} \tag{28}$$

where $\theta_{\mathrm{sq},f}$ and $\theta_{\mathrm{sq},b}$ are squint angles of forward and backward looks, respectively. Assuming that the magnitude of $\theta_{\mathrm{sq},f}$ is the same as that of $\theta_{\mathrm{sq},b}$ ($\theta_{\mathrm{sq}} \equiv \theta_{\mathrm{sq},f} = -\theta_{\mathrm{sq},b}$), we obtain the following expression by subtracting (27) from (28):

$$f_{\mathrm{dc},f} - f_{\mathrm{dc},b} = \frac{4v_{\mathrm{sat}} \sin\theta_{\mathrm{sq}}}{\lambda}. \tag{29}$$

Applying (29) to (26), we find

$$\Delta x_{\mathrm{iono}} = -\frac{v_g n T_c \lambda}{16\pi v_{\mathrm{sat}} \sin\theta_{\mathrm{sq}}} \frac{\partial \Delta\phi_{\mathrm{iono}}}{\partial \eta} \tag{30}$$

$nT_c$ in (30) can be interpreted as the passing time of the SAR satellite from the onset of the forward look to the end of the backward look. Thus, if the angle corresponding to the satellite arc length covered within $nT_c$ is denoted by $2\theta$, a simple geometrical relation gives us

$$v_{\mathrm{sat}} n T_c \approx 2\theta (r_{\mathrm{earth}} + h_{\mathrm{sat}}) \tag{31}$$

where $r_{\mathrm{earth}}$ is the radius of the earth. Combining (30) and (31) to eliminate $nT_c$, we find

$$\Delta x_{\mathrm{iono}} = -\frac{v_g \lambda (r_{\mathrm{earth}} + h_{\mathrm{sat}})\theta}{8\pi v_{\mathrm{sat}}^2 \sin\theta_{\mathrm{sq}}} \frac{\partial \Delta\phi_{\mathrm{iono}}}{\partial \eta}. \tag{32}$$

From a simple geometrical relation, we obtain the following approximated relation:

$$h_{\mathrm{sat}} \sin\theta_{\mathrm{sq}} \approx r_{\mathrm{earth}} \theta. \tag{33}$$

Applying (33) to (32)

$$\Delta x_{\mathrm{iono}} = -\frac{v_g \lambda h_{\mathrm{sat}} (r_{\mathrm{earth}} + h_{\mathrm{sat}})}{8\pi v_{\mathrm{sat}}^2 r_{\mathrm{earth}}} \frac{\partial \Delta\phi_{\mathrm{iono}}}{\partial \eta}. \tag{34}$$

Moreover, considering that

$$v_g = v_{\mathrm{sat}} \frac{r_{\mathrm{earth}}}{r_{\mathrm{earth}} + h_{\mathrm{sat}}}. \tag{35}$$

Equation (34) is rewritten as

$$\Delta x_{\mathrm{iono}} = -\frac{\lambda h_{\mathrm{sat}}}{8\pi v_{\mathrm{sat}}} \frac{\partial \Delta\phi_{\mathrm{iono}}}{\partial \eta}. \tag{36}$$

If the off-nadir angle corresponding to zero Doppler range ($R_0$) is denoted by $\theta_{\mathrm{off-nadir}}$, then we can approximate $h_{\mathrm{sat}}$ by $R_0 \cos\theta_{\mathrm{off-nadir}}$, that is

$$\Delta x_{\mathrm{iono}} \approx -\frac{\lambda R_0 \cos\theta_{\mathrm{off-nadir}}}{8\pi v_{\mathrm{sat}}} \frac{\partial \Delta\phi_{\mathrm{iono}}}{\partial \eta}. \tag{37}$$

From the relationship $x = \eta v_{\mathrm{sat}}$, we finally obtain

$$\Delta x_{\mathrm{iono}} = -\frac{\lambda R_0 \cos\theta_{\mathrm{off-nadir}}}{8\pi} \frac{\partial \Delta\phi_{\mathrm{iono}}}{\partial x}. \tag{38}$$

Comparing (38) and (1), we find (1) is equivalent to (38) when putting $h_{\mathrm{iono}}/h_{\mathrm{sat}} = \cos\theta_{\mathrm{off-nadir}}/2$. That is, (1) is more general expression for a relation between ionospheric azimuth offset and the ionospheric phase delay.

## ACKNOWLEDGMENT

Advanced Land Observing Satellite-2 (ALOS-2) data were provided under a cooperative research contract with the Japan Aerospace Exploration Agency (JAXA). The ownership of ALOS-2 data belongs to JAXA. Figures were generated using the Generic Mapping Tools (GMT) software package [34]. We used the Geospatial Information Authority of Japan (GSI) 10 m digital ellipsoidal height model (DEHM) Japan made from GSI 10 m-mesh digital elevation model (DEM) by Mikio Tobita. The authors appreciate deeply Hiroshi Munekane, Nic Donnelly, Chris Crook, Matthew Wightman, and the anonymous reviewers for reading carefully the article to give helpful comments on this article.

## REFERENCES

[1] R. Michel, J.-P. Avouac, and J. Taboury, "Measuring ground displacements from SAR amplitude images: Application to the landers earthquake," *Geophys. Res. Lett.*, vol. 26, no. 7, pp. 875–878, Apr. 1999, doi: 10.1029/1999GL900138.

[2] N. B. D. Bechor and H. A. Zebker, "Measuring two-dimensional movements using a single InSAR pair," *Geophys. Res. Lett.*, vol. 33, no. 16, Aug. 2006, Art. no. L16311, doi: 10.1029/2006GL026883.

[3] M. Tobita, M. Murakami, H. Nakagawa, H. Yarai, S. Fujiwara, and P. A. Rosen, "3-D surface deformation of the 2000 Usu eruption measured by matching of SAR images," *Geophys. Res. Lett.*, vol. 28, no. 22, pp. 4291–4294, Nov. 2001, doi: 10.1029/2001GL013329.

[4] Y. Himematsu and M. Furuya, "Fault source model for the 2016 Kumamoto earthquake sequence based on ALOS-2/PALSAR-2 pixel-offset data: Evidence for dynamic slip partitioning," *Earth, Planets Space*, vol. 68, p. 169, Oct. 2016, doi: 10.1186/s40623-016-0545-7.

[5] Y. Morishita, T. Kobayashi, S. Fujiwara, and H. Yarai, "Complex crustal deformation of the 2016 Kaikōura, New Zealand, Earthquake revealed by ALOS-2," *Bull. Seismolog. Soc. Amer.*, vol. 108, no. 3B, pp. 1746–1756, May 2018, doi: 10.1785/0120180070.

[6] S. Barbot, Y. Hamiel, and Y. Fialko, "Space geodetic investigation of the coseismic and postseismic deformation due to the 2003 Mw 7.2 Altai earthquake: Implications for the local lithospheric rheology," *J. Geophys. Res.*, vol. 113, no. B3, Mar. 2008, Art. no. B03403, doi: 10.1029/2007JB005063.

[7] I. J. Hamling *et al.*, "Complex multifault rupture during the 2016 Mw 7.8 Kaikōura earthquake, New Zealand," *Science*, vol. 356, no. 6334, Apr. 2017, Art. no. eaam7194, doi: 10.1126/science.aam7194.

[8] F. Casu, A. Manconi, A. Pepe, and R. Lanari, "Deformation time-series generation in areas characterized by large displacement dynamics: The SAR amplitude pixel-offset SBAS technique," *IEEE Trans. Geosci. Remote Sens.*, vol. 49, no. 7, pp. 2752–2763, Jul. 2011, doi: 10.1109/TGRS.2010.2104325.

[9] H.-S. Jung, W.-J. Lee, and L. Zhang, "Theoretical accuracy of along-track displacement measurements from multiple-aperture interferometry (MAI)," *Sensors*, vol. 14, no. 9, pp. 17703–17724, Sep. 2014, doi: 10.3390/s140917703.

[10] A. L. Gray, K. E. Mattar, and G. Sofko, "Influence of ionospheric electron density fluctuations on satellite radar interferometry," *Geophys. Res. Lett.*, vol. 27, no. 10, pp. 1451–1454, May 2000, doi: 10.1029/2000GL000016.

[11] T. Kobayashi, Y. Takada, M. Furuya, and M. Murakami, "Locations and types of ruptures involved in the 2008 Sichuan earthquake inferred from SAR image matching," *Geophys. Res. Lett.*, vol. 36, no. 7, Apr. 2009, Art. no. L07302, doi: 10.1029/2008GL036907.

[12] C. Liang and E. J. Fielding, "Measuring azimuth deformation with L-band ALOS-2 ScanSAR interferometry," *IEEE Trans. Geosci. Remote Sens.*, vol. 55, no. 5, pp. 2725–2738, May 2017, doi: 10.1109/TGRS.2017.2653186.

[13] U. Wegmuller, C. Werner, T. Strozzi, and A. Wiesmann, "Ionospheric electron concentration effects on SAR and INSAR," in *Proc. IEEE Int. Symp. Geosci. Remote Sens.*, Jul. 2006, pp. 3731–3734, doi: 10.1109/IGARSS.2006.956.

[14] P. He, Y. Wen, C. Xu, and Y. Chen, "High-quality three-dimensional displacement fields from new-generation SAR imagery: Application to the 2017 Ezgeleh, Iran, earthquake," *J. Geodesy*, vol. 93, no. 4, pp. 573–591, Apr. 2019, doi: 10.1007/s00190-018-1183-6.

[15] D. Raucoules and M. de Michele, "Assessing ionospheric influence on L-band SAR data: Implications on coseismic displacement measurements of the 2008 Sichuan earthquake," *IEEE Geosci. Remote Sens. Lett.*, vol. 7, no. 2, pp. 286–290, Apr. 2010, doi: 10.1109/LGRS.2009.2033317.
[16] J. S. Kim, "Development of ionosphere estimation techniques for the correction of SAR data," Ph.D. dissertation, Dep. Civil, Env., Geomatic Eng., ETH Zurich, Zurich, Switzerland, 2013.
[17] A. C. Chen and H. A. Zebker, "Reducing ionospheric effects in InSAR data using accurate coregistration," *IEEE Trans. Geosci. Remote Sens.*, vol. 52, no. 1, pp. 60–70, Jan. 2014, doi: 10.1109/TGRS.2012.2236098.
[18] R. Brcic, A. Parizzi, M. Eineder, R. Bamler, and F. Meyer, "Estimation and compensation of ionospheric delay for SAR interferometry," in *Proc. IEEE Int. Geosci. Remote Sens. Symp.*, Jul. 2010, pp. 2908–2911.
[19] F. J. Meyer, "Performance requirements for ionospheric correction of low-frequency SAR data," *IEEE Trans. Geosci. Remote Sens.*, vol. 49, no. 10, pp. 3694–3702, Oct. 2011, doi: 10.1109/TGRS.2011.2146786.
[20] G. Gomba, A. Parizzi, F. De Zan, M. Eineder, and R. Bamler, "Toward operational compensation of ionospheric effects in SAR interferograms: The split-spectrum method," *IEEE Trans. Geosci. Remote Sens.*, vol. 54, no. 3, pp. 1446–1461, Mar. 2016, doi: 10.1109/TGRS.2015.2481079.
[21] U. Wegmüller, C. Werner, O. Frey, C. Magnard, and T. Strozzi, "Reformulating the split-spectrum method to facilitate the estimation and compensation of the ionospheric phase in SAR interferograms," *Procedia Comput. Sci.*, vol. 138, pp. 318–325, Jan. 2018, doi: 10.1016/j.procs.2018.10.045.
[22] S. Fujiwara and M. Tobita, "SAR interferometry techniques for precise surface change detection," (in Japanese with English abstract), *J. Geodetic Soc. Jpn.*, vol. 45, no. 4, pp. 283–295, Dec. 1999, doi: 10.11366/sokuchi1954.45.283.
[23] M. Tobita, S. Fujiwara, M. Murakami, H. Nakagawa, and P. A. Rosen, "Accurate offset estimation between two SLC images for SAR interferometry," (in Japanese with English abstract), *J. Geodetic Soc. Jpn.*, vol. 45, no. 4, pp. 297–314, Dec. 1999, doi: 10.11366/sokuchi1954.45.297.
[24] M. Tobita, "Development of SAR interferometry analysis and its application to crustal deformation study," (in Japanese with English abstract), *J. Geodetic Soc. Jpn.*, vol. 49, no. 1, pp. 1–23, Mar. 2003, doi: 10.11366/sokuchi1954.49.1.
[25] Y. Morishita, "A systematic study of synthetic aperture radar interferograms produced from ALOS-2 data for large global earthquakes from 2014 to 2016," *IEEE J. Sel. Topics Appl. Earth Observ. Remote Sens.*, vol. 12, no. 7, pp. 2397–2408, Jul. 2019, doi: 10.1109/JSTARS.2019.2921664.
[26] U. Wegmüller and C. L. Werner, "Gamma SAR processor and interferometry software," in *Proc. 3rd ERS Sci. Symp.*, Mar. 1997, pp. 1687–1692.
[27] C. Werner, U. Wegmüller, T. Strozzi, and A. Wiesmann, "Precision estimation of local offsets between pairs of SAR SLCs and detected SAR images," in *Proc. IEEE Int. Geosci. Remote Sens. Symp. (IGARSS)*, Jul. 2005, pp. 4803–4805, doi: 10.1109/IGARSS.2005.1526747.
[28] T. Hobiger and N. Jakowski, "Atmospheric signal propagation," in *Springer Handbook of Global Navigation Satellite Systems*, 1st ed. Cham, Switzerland: Springer, 2017, pp. 165–193.
[29] H. Sato, J. S. Kim, N. Jakowski, and I. Häggström, "Imaging high-latitude plasma density irregularities resulting from particle precipitation: Spaceborne L-band SAR and EISCAT observations," *Earth, Planets Space*, vol. 70, no. 1, pp. 1–8, Oct. 2018, doi: 10.1186/s40623-018-0934-1.
[30] B. Miyahara *et al.*, "Detection of ground surface deformation caused by the 2016 Kumamoto earthquake by InSAR using ALOS-2 data," *Bull. Geospatial Inf. Authority Jpn.*, vol. 64, pp. 21–26, Dec. 2016.
[31] S. Toda, H. Kaneda, S. Okada, D. Ishimura, and Z. K. Mildon, "Slip-partitioned surface ruptures for the Mw 7.0 16 April 2016 Kumamoto, Japan, earthquake," *Earth, Planets Space*, vol. 68, no. 1, Nov. 2016, doi: 10.1186/s40623-016-0560-8.
[32] P. He, Y. Wen, C. Xu, and Y. Chen, "Complete three-dimensional near-field surface displacements from imaging geodesy techniques applied to the 2016 kumamoto earthquake," *Remote Sens. Environ.*, vol. 232, Oct. 2019, Art. no. 111321, doi: 10.1016/j.rse.2019.111321.
[33] T. Motohka, Y. Kankaku, S. Miura, and S. Suzuki, "ALOS-4 L-band SAR mission and observation," in *Proc. IEEE Int. Geosci. Remote Sens. Symp. (IGARSS)*, Jul. 2019, pp. 5271–5273, doi: 10.1109/IGARSS.2019.8898169.
[34] P. Wessel and W. H. Smith, "New, improved version of generic mapping tools released," *EOS Trans. Amer. Geophys. Union*, vol. 79, p. 579, Nov. 1998.

**Tatsuya Yamashita** received the master's and the Ph.D. degrees in cosmosciences from Hokkaido University, in 2009 and 2014, respectively. In his Ph.D. study, he mainly worked on atmospheric convection systems under early Mars-like conditions.

Since 2014, he has been with the Geospatial Information Authority of Japan, Tsukuba, Japan. In 2019, he was a Visiting Researcher with Land Information New Zealand, Wellington, New Zealand. His research interests include application of synthetic aperture radar and global navigation satellite systems to maintenance of a national geodetic datum.

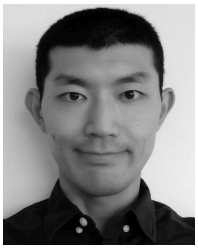

**Yu Morishita** received the B.S. and Ph.D. degrees in geophysics from Hokkaido University, Sapporo, Japan, in 2008 and 2016, respectively.

Since 2008, he has been with the Geospatial Information Authority of Japan, Tsukuba, Japan. In 2012, he was a Guest Researcher with the Delft University of Technology, Delft, The Netherlands. From 2018 to 2020, he was a Visiting Researcher with the University of Leeds, Leeds, U.K., supported by the Japan Society for the Promotion of Science Overseas Research Fellowship. His research interests include the development of synthetic aperture radar (SAR) data analysis techniques and their application to surface deformation monitoring.

Dr. Morishita was a recipient of the Second Prize for the Young Scientist Award at the 2013 Asia–Pacific Conference on SAR.

**Tomokazu Kobayashi** received the B.S. degree in geophysics from Tohoku University, Sendai, Japan, in 1999, and the M.A. degree in arts and sciences and the Ph.D. degree in geophysics from The University of Tokyo, Tokyo, Japan, in 2001 and 2004, respectively.

He is currently the Head of Space Geodesy Research Division, Geospatial Information Authority of Japan, Tsukuba, Japan. He has studied ground deformation caused by geohazards such as seismic and volcanic activities with an interferometric synthetic aperture radar (SAR). His research interest includes the development of SAR-based application techniques for detecting ground deformation.